HyLink: Towards High Throughput LPWANs with LoRa Compatible Communication

Xianjin Xia, Qianwu Chen, Ningning Hou, Yuanqing Zheng

The Hong Kong Polytechnic University, Hong Kong, China

{xjxia,qwchen,ning2hou,yqzheng}@polyu.edu.hk

ABSTRACT

This paper presents the design and implementation of HyLink which aims to fill the gap between limited link capacity of LoRa and the diverse bandwidth requirements of IoT systems. At the heart of HyLink is a novel technique named *parallel Chirp Spread Spectrum* modulation, which tunes the number of modulated symbols to adapt bit-rates according to channel conditions. Over strong link connections, HyLink fully exploits the link capability to transmit more symbols and thus transforms good channel SNRs to high link throughput. While for weak links, it conservatively modulates one symbol and concentrates all transmit power onto the symbol to combat poor channels, which can achieve the same performance as legacy LoRa. HyLink addresses a series of technical challenges on encoding and decoding of multiple payloads in a single packet, aiming at amortizing communication overheads in terms of channel access, radio-on power, transmission air-time, *etc.* We perform extensive experiments to evaluate the effectiveness of HyLink. Evaluations show that HyLink produces up to 10× higher bit rates than LoRa when channel SNRs are higher than 5 dB. HyLink inter-operates with legacy LoRa devices and can support new emerging traffic-intensive IoT applications.

CCS CONCEPTS

• **Networks → Link-layer protocols**.

KEYWORDS

Internet of Things, LPWAN, LoRa, throughput, adaptive data rate

1 INTRODUCTION

Recent years have witnessed a trend to connect Internet-of-Things (IoTs) using Low-Power Wide-Area Network (LPWAN) technologies such as NB-IoT [54, 61], LoRa [32, 34, 48, 49] and Sigfox [46]. The number of global LPWAN connections grows explosively in the

past five years (2016–2021) with an annual rate of 89.3 % [25, 35]. LPWANs are featured with both long-range and low-power, outperforming traditional IoT technologies in terms of coverage, scalability and costs [11, 25, 47].

LoRa adopts a prominent Chirp Spread Spectrum (CSS) modulation technology. The PHY bit rates of a LoRa radio range from 0.018 kbps to 37.5 kbps depending on the radio configurations [42]. Restricted by the low duty-cycle regulation of ISM band (*e.g.*, ≤1 % in LoRaWAN [34]), the effective data rate of a LoRaWAN link can be much lower (*e.g.*, a few bps). As such, LoRa is mainly adopted in IoT scenarios that transmit low-volume and infrequent traffics (*e.g.*, environment monitoring [14, 28], smart metering [26]).

However, in practice, the traffic requirements of an IoT system can be diverse and ever-changing. For instance, a fire-alarm application normally produces low traffics yet generates bursty traffics, including video streaming of on-site cameras, upon detecting abnormal events, which requires high throughput. Besides, a practical IoT system may consist of not only low-volume IoT traffics in a few bps, but also a variety of traffic-intensive system services hungry for bandwidth (*e.g.*, firmware update over-the-air [43]). Latest IoT applications use multi-modal sensors to acquire rich data representations (*e.g.*, text, voice, image, *etc.*), which calls for high throughput data collection over wide areas.

Unfortunately, LoRa does not provide sufficient link capacity to support traffic-intensive tasks even over relatively good wireless channels. The limited throughput may prevent a link from serving regular IoT traffics let alone those need higher throughput. Moreover, due to the slow link speed, it needs to turn on LoRa radio for a rather long time, which consumes lots of power and dramatically shortens the battery life. The limited link capacity has indeed become a major factor hindering the wider adoption and development of LoRa in practical IoT systems. Our study aims to fill the gap by bringing high throughput to LPWAN links without sacrificing communication range or consuming extra power.

We revisit LoRa PHY to seek potential improving rooms for link throughput. We find that the current LoRa adopts narrow-band modulation and long symbols to support reliable communications at long-range and low-power. Such PHY designs are beneficial for combating the probable bad channel conditions in the presence of long-range link connections. However, narrow-band and long symbol designs inevitably suffer slow rates of symbol modulation, which can physically restrict link capacity. As a consequence, the maximum throughput of a link connection is confined to a few kbps even when a link has very good channel conditions. While it is reasonable to transmit at conserved data rates through weak link connections, *can we fully exploit the channel capability of strong links to break the limitations of LoRa PHY for higher throughput?* We argue that rather than transmitting one symbol at a time as

Figure 1: Parallel CSS (p-CSS) enlarges modulation space and produces near $N\times$ bit-rate gains.

Figure 2: (a,b) Spectra of CSS and p-CSS signals; (c,d) Modulated symbols of CSS and p-CSS ($N = 4$) in a chirp duration.

LoRa does, links of strong connections could be better utilized by transmitting multiple symbols concurrently, which is promising to multiply throughput by times.

To fully harness the wireless channel conditions, we propose a novel parallel CSS technique (termed *p-CSS*) which modulates N symbols in a chirp duration to speed up bit rates over strong links. While N symbols are modulated, the chirps of different symbols would generally differ in frequency, which enables us to demodulate the symbols in parallel. From a signal modulation perspective, p-CSS can dramatically increase symbol modulation space. As illustrated in Figure 1, the standard CSS divides a frequency band into M bins and selects one out of the M bins to modulate a symbol. The modulation space is M. If a second symbol is modulated in the same spectrum, the modulation space can be increased to $M \times (M - 1)$, which allows extra $\log_2(M - 1)$ bits to be carried in the same chirp duration. p-CSS can produce near $N\times$ gains when N symbols are modulated simultaneously.

p-CSS preserves the benefits of LoRa (*e.g.*, long-range, low-power, high concurrency and good scalability), and goes beyond with high throughput in good channels. p-CSS can tune the number of modulated symbols to adapt PHY bit-rate according to the channel conditions of link connections. For strong link connections, p-CSS can fully use the link capability to concurrently transmit more symbols and thus transform good channel conditions to high throughput. Whereas for link connections with poor channel conditions, p-CSS can conservatively modulate one symbol and concentrate all transmit power on the symbol to achieve the same performance of legacy LoRa. Empirical results show that p-CSS is able to bring bit-rate and power-efficiency improvements to most practical LoRaWAN links. As shown in Figure 2, we can send four symbols in parallel even when the channel SNR is −5 dB, which gives 3× higher bit-rates. A higher bit-rate empowers a link to transmit the same amount of data in a shorter time, which can reduce the active duration of IoT sensors and increase battery life by times.

Armed with p-CSS in the PHY, we further present a cross-layer extension for LoRa, *i.e.*, named *HyLink*. HyLink takes application data as input and modulates N symbols per chirp duration as p-CSS signals. To remain backward-compatible with legacy LoRa, HyLink divides payload data into N sub-groups and reuses LoRa encoders to encode data for each group. At a high level, HyLink works as if N LoRa payloads are carried in one packet. As such, LoRa packet can be regarded as a special case of HyLink packet when $N = 1$, which allows legacy LoRa devices to seamlessly communicate to a HyLink gateway. Moreover, as N payloads are transmitted through
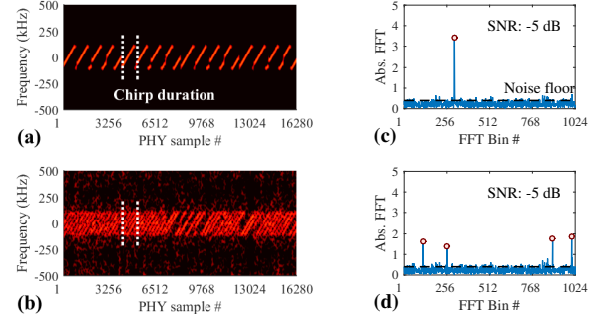
a single packet communication, they share the spectrum air-time and packet overheads (*e.g.*, packet preamble, sync. words, network ID), which can increase both link throughput and power efficiency without violating the ISM duty-cycle constraint for LoRaWAN.

We solve a series of technical challenges to turn HyLink into practice. Firstly, as the symbols of N payloads are modulated together in PHY, a receiver cannot separate the interleaved symbols of different payloads to correctly decode the payload symbols. To solve the problem, HyLink reuses the phase and amplitude of chirp signals, which are not modulated by standard CSS, to encode additional bits to uniquely identify the payload group of a symbol. At a receiver side, HyLink demodulates concurrent symbols and recovers the *phase and amplitude signatures* of chirp signals to distinguish symbols for different payloads.

However, it remains challenging to recover the encoded phase and amplitude signatures of p-CSS symbols, since the phase and amplitude can be severely distorted in wide-area communications. HyLink leverages the symbol structures of p-CSS signals to aggregate signal power into a few frequency bins of demodulated symbols, and extract phase and amplitude from the power-strengthened signals in the frequency domain. HyLink presents novel methods that exploit the frame structure of a packet to remove the impacts of channels on received p-CSS signals (*e.g.*, CFO, STO [57]). After that, we can correctly extract the phase and amplitude signatures of received p-CSS symbols.

Second, as p-CSS modulates symbols of N payloads in the same chirp duration, interference may happen among the symbols, which can distort the phase and amplitude signatures of symbols. HyLink exploits the bit-error tolerance of LoRa coding schemes to rearrange nearby symbols with sufficient frequency guards. Besides, we design heuristic strategies to allocate power resources among p-CSS symbols to ensure reliable communications of N payloads. Lastly, we devise a rate adaptation scheme for HyLink which tunes N (*i.e.*, the number of modulated symbols in p-CSS) to adapt PHY data rates to channel conditions.

We implement a prototype system of HyLink using Software Defined Radio (SDR) platforms and build a testbed consisting of both USRPs and off-the-shelf commodity LoRa nodes. We conduct extensive experiments to evaluate HyLink indoors and outdoors with more than 100 LoRaWAN links. Evaluations show that HyLink can carry more than 10 payloads in a packet. The PHY bit rates can reach up to 1 Mbps when SNRs $\geq$ 5 dB. As compared to standard LoRa, HyLink increases link throughput and, in the meanwhile,

decreases per-bit energy consumption by one order of magnitude. HyLink can inter-operate with legacy LoRa nodes and support concurrent communication with orthogonal parameters.

2 BACKGROUND AND MOTIVATION

Chirp Spread Spectrum. LoRa adopts Chirp Spread Spectrum (CSS) modulation in PHY, where a chirp signal spreads frequency across a given frequency band with bandwidth BW. The instantaneous frequencies of a chirp increase (*up-chirp*) or decrease (*down-chirp*) with time. A chirp with an increasing frequency from $-\frac{BW}{2}$ to $\frac{BW}{2}$ is called a *base chirp*. CSS changes the initial frequency of base chirp to modulate symbols. LoRa divides the whole frequency band into M bins and pre-defines M up-chirps starting with different frequency bins as a symbol set for modulation. Each symbol encodes $SF = \log_2 M$ bits, where SF corresponds to the *Spreading Factor* of CSS modulation. The procedure of LoRa modulation can be represented as follows.

$$S(f_{sym}, t) = e^{j2\pi(\frac{k}{2}t - \frac{BW}{2})t} \cdot e^{j2\pi f_{sym}t} = C(t) \cdot e^{j2\pi f_{sym}t} \quad (1)$$

where $C(t) = e^{j2\pi(\frac{k}{2}t - \frac{BW}{2})t}$ denotes a base chirp, k is the frequency increasing rate of base chirp and f_{sym} is a modulated frequency corresponding to the symbol.

LoRa demodulates a chirp signal by multiplying the chirp with the conjugate of base chirp, denoted by $C^{-1}(t)$. This procedure is called *de-chirp* and represented as below.

$$S(f_{sym}, t) \cdot C^{-1}(t) = e^{j2\pi f_{sym}t}. \quad (2)$$

A Fast Fourier Transform (FFT) on the dechirped signal gives f_{sym} which represents the encoded symbol data.

LoRa data-rate. PHY bit-rate refers to the number of bits physically transferred by a radio per second. The bit-rate of a LoRa radio can be primarily controlled by the Spreading Factor (SF) and signal bandwidth (BW) parameters of CSS modulation. Small SF and large BW modulate symbols with short chirp duration and air-time, which can be transmitted at faster speed and produce high bit-rates. A commodity LoRa radio (*e.g.*, Semtech SX1276 [42]) allows to configure SF in 6~12 and BW in 7.8~500 kHz. The bit-rate varies from 0.018 kbps to 37.5 kbps. The latest LoRa radio (*e.g.*, SX1280 [44]) increases bandwidth (*e.g.*, 2.4 MHz) and supports PHY bit-rate up to 254 kbps at higher power consumption and more radio resources (*e.g.*, wide frequency band, high-cost hardware, *etc.*).

As LoRaWAN operates in ISM bands (*e.g.*, 868 MHz in Europe and 915 MHz in US), a LoRaWAN link is restricted by the duty cycle regulations of ISM bands. For instance, the maximum duty cycle of the US 915 MHz band is 1 %, meaning that a LoRa radio shall transmit at most 36 seconds per hour [40]. The effective data rate of a LoRaWAN link can be much lower than the PHY bit-rate of a LoRa radio in practice.

Need for high link throughput. LoRa and other LPWAN technologies are designed for low-power wide-area IoT connections, where the IoT sensors normally transmit low-volume traffic infrequently (*e.g.*, a few messages a day). However, many emerging applications need multi-modal sensors to acquire rich data representations including images and videos, which calls for high-throughput links to collect large-volume sensory data over wide areas. For instance, the latest fire-alarm systems may not only need

conventional heat and smoke detector readings, but also require camera shots of target venues to detect potential fire risks [7]. Even for a low-traffic IoT scenario like environment monitoring and smart metering, practical systems may still need various traffic-intensive services. For example, firmware update over-the-air is a critical function specified by LoRaWAN to support on-site system upgrade for millions of IoT devices [34, 43]. However, it would take a rather long time (*e.g.*, tens of minutes to a few hours) to distribute a image file in hundreds of kB with LoRaWAN, which can be time-consuming and power-hungry [20]. The current LoRaWAN cannot support bulk data transmission effectively due to constraints of link throughput. HyLink aims to fill this gap by empowering LoRaWANs with high throughput to support traffic-intensive applications.

3 PARALLEL CSS (P-CSS)

LoRa adopts two specific designs, *i.e.*, *narrow-band CSS modulation* and *long symbols*, that allow transmitted chirp signals to be received with high sensitivity even after a long distance transmission (*e.g.*, down to −148 dBm [42]). The longest LoRa communication range can reach hundreds of kilometers [55], thanks to the excellent PHY designs. On the other hand, such designs inevitably suffer slow rates of symbol modulation, which physically restricts link capacity. The highest data rate of a LoRa link is limited to a few kbps regardless of channel conditions of a physical link. While it is reasonable for LoRa to communicate at conserved data rates to combat the potentially poor channels experienced by distant link connections, can we transmit with higher rates over a long communication range at low power consumption when a link has good SNRs?

LoRa supports Adaptive Data Rates (ADR). When a link has good SNRs, CSS modulation can be configured with small Spreading Factors (SFs) which modulate symbols in short time duration and produce high data rates. However, a LoRa symbol cannot be too short due to constraints of communication reliability. The throughput improvement of LoRa ADR is very limited in practice.

We propose a parallel CSS technique (*i.e.*, p-CSS) that concurrently modulates N symbols in a chirp duration to multiply bit rates for links in good SNRs. p-CSS signals share benefits of LoRa communications such as high Rx sensitivity, low power, high concurrency, *etc.* As N symbols are transmitted over the same frequency with the same air-time, it can increase link throughput without violating the duty-cycle constraints or consuming extra spectrum resources.

While p-CSS modulates N symbols in the same chirp duration, the chirp signals of N symbols superimpose in time domain. We can use a standard CSS demodulation algorithm given by Eq.(2) to demodulate p-CSS signals, which will produce N frequency components corresponding to N concurrent symbols. Unlike existing parallel decoding studies (*e.g.*, FTrack[59], CIC [45], PCube [57]) that demodulate concurrent symbols from random packet collisions, p-CSS is able to arrange concurrent symbols in a way that facilitates parallel decoding, which makes parallel decoding easier and more robust. In doing so, p-CSS deals with new design issues such as how to decide the number of symbols modulated in parallel, how to properly put concurrent symbols in PHY, and how to allocate resources among concurrent symbols.

In practice, p-CSS can be used as an enhancement for the current LoRa PHY. We can upgrade legacy LoRaWANs to improve throughput performance for some links when channel SNRs are
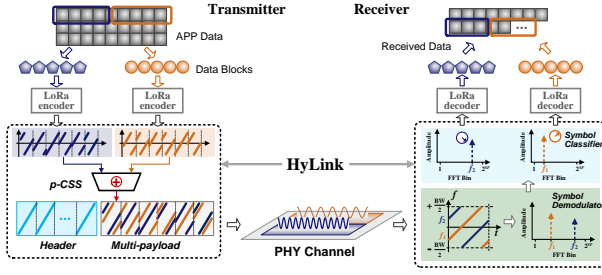
Figure 3: HyLink workflow.

good enough. The number of modulated symbols (*i.e.*, N) acts as a parameter for tuning data rates of p-CSS modulation. We can choose a large N for high data rate when a physical link offers high SNRs. If a link is of long-distance or poor SNRs, we can modulate fewer symbols to ensure good reliability of communications. When N decreases to 1, p-CSS turns into a standard LoRa that can transmit to the longest range at the lowest data-rates. Essentially, p-CSS introduces a new dimension, orthogonal to existing LoRa ADR, for adapting link throughput according to channel SNRs.

4 HYLINK DESIGN

4.1 Overview

HyLink uses p-CSS in PHY to provide high data rates for strong LPWAN link connections. HyLink develops novel techniques to support parallel encoding and decoding of multiple payloads in a single HyLink packet, while maintaining good compatibility with legacy LoRa. As illustrated in Figure 3, HyLink takes data from upper-layer applications as input, and then divides the data into smaller blocks. Each data block is called a *payload group*. HyLink reuses a standard LoRa encoder to encode data of each payload group into PHY symbols. The symbols from different payloads will be tagged with unique PHY signatures as *payload IDs* (§4.2). After that, HyLink feeds symbols of N payloads into PHY to modulate as p-CSS signals and prepends with a packet header before transmitting on a physical channel. At a receiver side, HyLink demodulates p-CSS signals and recovers payload IDs of concurrent symbols to classify symbols into corresponding payload groups. The separated symbols of N payloads are decoded by N LoRa decoders in parallel to complete the decoding of a HyLink packet.

At a high level, HyLink acts as if N LoRa payloads are carried in a single packet. The overheads in terms of packet header (*e.g.*, preamble, SFD), channel access (*e.g.*, channel detection, back-off, *etc.*) and transmission air-time can be effectively amortized over N payloads. It can increase communication throughput and per-bit power efficiency without violating the duty cycle regulations of LoRaWAN. Basically, a legacy LoRa packet can be considered as a special case of HyLink packet when $N = 1$. HyLink gateways are backward-compatible and can receive packets from deployed legacy LoRa devices. In the following, we will present the design of HyLink in details.

4.2 PHY (De)Modulation for Multi-payload

In this subsection, we focus on how to modulate and demodulate symbols of N payloads in PHY.

Multi-payload modulator. HyLink uses p-CSS to modulate symbols of N payloads in PHY. The signals of N payloads will be concurrently transmitted and superimpose in the air. A receiver can demodulate received p-CSS signals to get all concurrent symbols. However, as symbols of N payloads interleave together, a receiver is incapable of distinguishing which symbol belongs to which payload, which can prevent parallel decoding of the N payloads.

A basic idea is to add PHY signatures (*e.g.*, distinctive phase and amplitude features) to the modulated chirps to explicitly identify the payload groups of corresponding symbols, *i.e.*, termed *payload IDs*. We notice that standard CSS only uses the initial frequency of a chirp to modulate a symbol but ignores the phase and amplitude of the chirp. As such, we can modulate the phase and amplitude of chirp signals into distinctive PHY signatures to indicate payload IDs of modulated symbols. Formally, we represent the modulated p-CSS signals of N symbols as below.

$$x(t) = \sum_{i=1}^{N} \underbrace{(\alpha_i \cdot e^{j\phi_i})}_{\text{Payload ID: } \gamma_i,} \cdot \underbrace{S(f_{sym}(i), t)}_{\text{Symbol of payload } \#i} , \qquad (3)$$

where $S(f_{sym}(i), t)$ denotes the symbol of the ith payload, $\gamma_i = \alpha_i \cdot e^{j\phi_i}$ is the payload ID, α_i and ϕ_i are the amplitude and phase signatures modulated on p-CSS signals. A receiver can decode payload IDs (*i.e.*, γ_i) by extracting the phase and amplitude signatures from received p-CSS signals, and rely on the payload IDs to classify symbols to different payload groups.

A primary concern, however, is about the reliability of payload ID detection. Note that p-CSS signals are specifically used for long-range communications. A weak chirp signal can be received with high sensitivity (*e.g.*, below noise floor) and still get demodulated correctly. However, the chirp's phase and amplitude may not be detected reliably from the received signals due to impacts of noises.

Fortunately, thanks to the long chirp duration of PHY symbols, the demodulation of a chirp can accumulate power of all signal samples into a single frequency bin, while spreading noise power over the whole spectrum due to the random natures of noises. As shown in Figure 4, though the raw chirp signals are overwhelmed by noises, the accumulated power of signal samples can become high above the noise floor because of the *power accumulation effect*. We can rely on this power-strengthened frequency peak to extract phase and amplitude of the original chirp. In Figure 5, we see that the phase and amplitude of chirp signals can be reliably detected from their demodulated frequencies even when the raw signals are weaker than noises (*e.g.*, SNR<−5 dB). Moreover, a receiver can easily increase sampling rates to receive more samples of a chirp signal. The frequency peak in Figure 4(c) is expected to increase as more samples are being accumulated whereas noise power increases much slower, which can increase phase and amplitude detection accuracy as shown in Figure 5(b).

Multi-payload demodulator. While p-CSS signals transmit through a physical channel, the communication channel can distort the frequency, phase and amplitude of received signals. Though we can use a standard CSS demodulation algorithm to demodulate concurrent symbols from received p-CSS signals, how to correctly recover the payload IDs of received symbols remains a big problem.
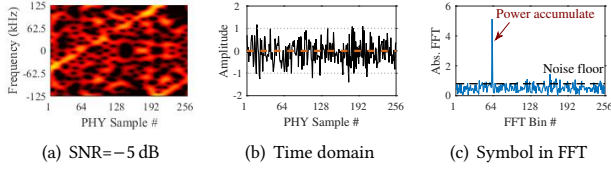
(a) SNR=−5 dB (b) Time domain (c) Symbol in FFT

Figure 4: (a,b) Raw chirp signals in frequency and time domains, (c) The signal power of PHY samples are accumulated during chirp demodulation.

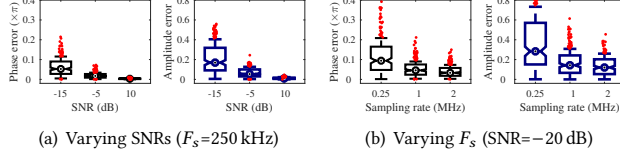(a) Varying SNRs (F_s=250 kHz) (b) Varying F_s (SNR=−20 dB)

Figure 5: Accuracy of phase/amplitude detection under (a) different SNRs and (b) Receiver sampling rates (F_s).

Without loss of generality, we represent a received p-CSS signal as follows.

$$y(t) = h \cdot e^{-j(2\pi \Delta f_{cfo} t + \varphi_{osc})} \cdot \sum_{i=1}^{N} \gamma_i S(f_{sym}(i), t + \Delta t_{sto}) + n(t), \quad (4)$$

where h represents the phase and amplitude impacts of a channel, Δf_{cfo} characterizes Carrier Frequency Offset (CFO) and φ_{osc} denotes oscillator phase offset between transmitter and receiver, Δt_{sto} is STO (i.e., time gap between signal arrival and being sampled by a receiver) [57], and $n(t)$ denotes noises. Our goal is to recover the payload IDs of payload symbols (i.e., γ_i). Now, the problem becomes how to remove the impacts of channel (h), CFO (Δf_{cfo}) and STO (Δt_{sto}) to extract a clear γ_i from $y(t)$.

Initially, we try to use existing calibration methods for LoRa [6, 57] to estimate channel, CFO and STO respectively, and remove their impacts from received p-CSS signals. We use the method presented in [6] to calibrate received p-CSS signals of a HyLink packet and extract the phase and amplitude of received symbols from the calibrated p-CSS signals. Figure 6(a,b) present the measurement results of a HyLink packet with two payloads. We expect to get stable phase and amplitude measurements from different symbols of the two payloads. Unfortunately, the measured phase and amplitude vary across symbols. They deviate randomly from their true values, i.e., the encoded phase and amplitude signatures of each payload.

According to [6, 57], the inter-symbol variances of phase and amplitude measurements can be caused by STO. STO would introduce both frequency shift and phase rotations to a received chirp signal, where the phase rotation is characterized by $\varphi_{sto} = 2\pi f_{sym} \Delta t_{sto}$. Although Δt_{sto} remains invariant throughout the reception of a packet, φ_{sto} would still vary across symbols because different symbols differ in f_{sym}. Moreover, as the chirp signal of a symbol generally consists of two parts (i.e., the first sub-chirp from f_{sym} to $\frac{BW}{2}$ and the second from $-\frac{BW}{2}$ to f_{sym}), STO also adds heterogeneous phase rotations to the two sub-chirps. It can lead to incoherent combining of signal power while we use all samples of the symbol for amplitude measurement. This explains why the measured amplitude can be lower than the encoded amplitude and vary across
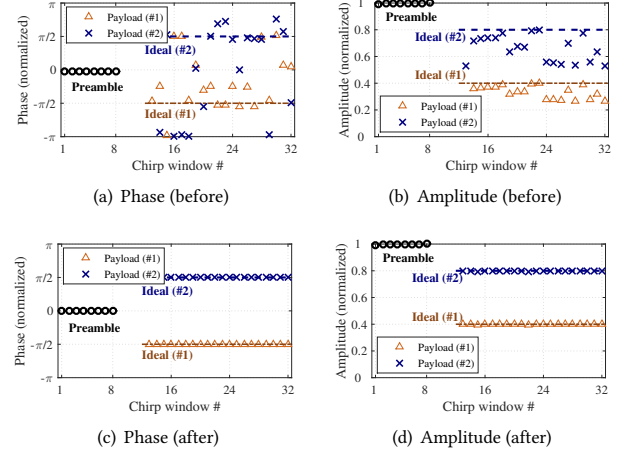

(a) Phase (before) (b) Amplitude (before)

(c) Phase (after) (d) Amplitude (after)

Figure 6: Phase and amplitude signature detection using (a,b) existing calibration methods; and (c,d) our method.

symbols (see Figure 6(b)). In summary, STO can distort the phase and amplitude of different symbols heterogeneously which cannot be removed by existing calibration methods in literature.

To handle the problem, we present a novel method that exploits the frame structure of HyLink packet as well as the symbol structures of received p-CSS signals to reliably extract payload IDs for p-CSS symbols. To be specific, as we prepend the modulated p-CSS signals of HyLink payloads with a LoRa packet header (i.e., preamble, sync. words and SFD), the chirp signals of packet header are tagged with a payload ID $\gamma = 1$ (i.e., phase 0°, amplitude 1). Our key insight is that as the signals in packet header and payload are traversing through the same communication channel, they are likely to experience the same CFO, STO and channel impacts. Thus, we can use a received preamble base-chirp to reconstruct the received signals of any payload symbols, including the symbol-dependent phase and amplitude distortions, based on the CSS modulation principle. In particular, consider a received symbol of the ith payload representing as below.

$$y_i(t) = h \cdot e^{-j(2\pi \Delta f_{cfo} t + \varphi_{osc})} \cdot \gamma_i \cdot S(f_{sym}(i), t + \Delta t_{sto}). \quad (5)$$

The signals of the same symbol (i.e., $f_{sym}(i)$) reconstructing from a received preamble would be as follows.

$$y_i^{pre}(t) = h \cdot e^{-j(2\pi \Delta f_{cfo} t + \varphi_{osc})} \cdot \gamma_{pre} \cdot S(f_{sym}(i), t + \Delta t_{sto}), \quad (6)$$

where $\gamma_{pre} = 1$ is the payload ID of preamble chirps. Comparing (5) and (6), we find that the two signals differ only in payload IDs (i.e., γ_i and γ_{pre}). Thus, we can conjugate multiply (5) and (6) to derive the payload ID of the symbol (i.e., γ_i), which can be represented in the following.

$$y_i(t) \cdot [y_i^{pre}(t)]^* = \gamma_i. \quad (7)$$

In Eq.(7), the reconstructed signal copy of a symbol (i.e., $y_i^{pre}(t)$) is used as a *mask* for payload ID extraction. Note that the frequency of a symbol (i.e., $f_{sym}(i)$) is required to create a mask. In practice, we need to first demodulate $y_i(t)$ to get $f_{sym}(i)$ and next use the symbol frequency to build a mask for payload ID extraction. Figures 6(c) and (d) present the results of mask-based payload ID detection.
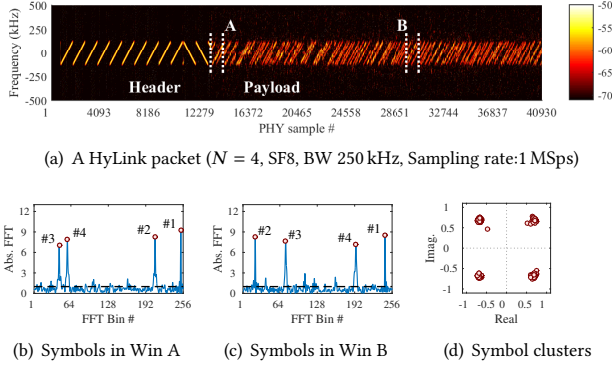
(a) A HyLink packet (N = 4, SF8, BW 250 kHz, Sampling rate:1 MSps)

(b) Symbols in Win A   (c) Symbols in Win B   (d) Symbol clusters

Figure 7: (a) Received signals of a HyLink packet (N=4); (b,c) Symbols in windows A, B and their payload groups; (d) The signatures of symbols form four clusters.

We see that the detected phase and amplitude signatures match well with their true values.

Putting all together. We use a case study to demonstrate the PHY operations of HyLink. We setup $N = 4$ payload groups and configure p-CSS modulation with SF8 and BW 250 kHz. The sampling rate of receiver is 1 MSps. Figure 7(a) displays the spectrogram of a received HyLink packet. We can clearly see that more than one chirp are modulated in the same chirp duration in the payload part, indicating a high utilization of the spectrum.

A HyLink receiver reuses the packet detection algorithm of LoRa to detect packet header as well as the frame timing (*i.e.*, symbol edges), and next demodulates the symbols in the payload. We can demodulate four symbols from each chirp window as shown in Figure 7(b,c). HyLink extracts the phase and amplitude signatures of received symbols to recover their payload IDs. Figure 7(d) presents the phase and amplitude of all symbols in the same I-Q diagram. We see that the symbols form 4 clusters. Symbols in each cluster belong to the same payload. HyLink can accordingly separate the symbols of different payloads. Finally, HyLink feeds the classified payload symbols to four LoRa decoders for parallel decoding to finish the reception of a HyLink packet.

4.3 Handling Inter-payload Interference

As symbols of N payloads are modulated concurrently in a chirp duration, interference may happen among these collocating symbols (*i.e.*, termed *inter-payload interference*). For instance, Figure 8(a) displays the modulated p-CSS signals of three symbols (*i.e.*, free of CFO, STO and noises). By demodulating the signals, we expect an ideal result where three symbols appear only in their corresponding FFT bins and the other bins are left clear. However, the frequencies of demodulated symbols appear not only in their expected FFT bins but also in adjacent bins (*i.e.*, side lobes) as shown in Figure 8(c). Unexpected power spikes also appear in FFT bins that were supposed to be clear. Since the signals in Figure 8 are free of noises and channel distortions, these power spikes are primarily caused by inter-payload interference. We can observe more spikes as more symbols are modulated concurrently.

Inter-payload interference can affect HyLink communication in two aspects: First, the side lobes of collocating symbols are likely to
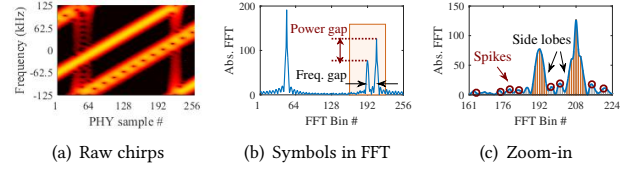

(a) Raw chirps   (b) Symbols in FFT   (c) Zoom-in

Figure 8: Inter-payload interference happens when modulating multiple symbols in PHY.

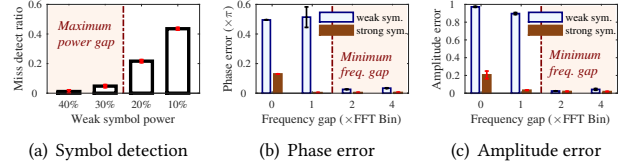(a) Symbol detection   (b) Phase error   (c) Amplitude error

Figure 9: (a) Miss detection of weak symbols in various power settings (normalized to the power of strong symbol); (b,c) Errors of phase and amplitude detection in various frequency gaps (weak symbol power: 40 %).

overlap if the symbols are close in frequency, *i.e.*, small frequency gap as shown in Figure 8(c). If the signal power of a symbol is weaker than that of collocating symbols, the weak symbol is likely to be submerged by the side lobes of strong symbols, resulting in *miss detection of weak symbols*. Second, inter-payload interference can distort the phase and amplitude signatures (*i.e.*, encoded payload IDs) of collocating symbols. In a special case when different payload groups share data bits, their PHY symbols appear in the same FFT bin (*i.e.*, *symbol collision*) and the symbol signatures suffer the most serious interference, which can lead to *incorrect payload decoding*. According to our measurement studies reported in Figure 9, we find that: (1) Weak symbols can be missed if the power is lower than 30 % of collocating symbols; (2) The phase and amplitude of weak symbols are highly distorted when a strong symbol is encoded nearby (*e.g.*, ≤ 1 FFT bin). Yet the interference becomes negligible as frequency gaps are large (*e.g.*, ≥2 FFT bins).

Enhanced HyLink encoder. To mitigate the impacts of inter-payload interference, we propose an enhanced encoder that can safeguard p-CSS modulated symbols with proper gaps in frequency and power. The enhanced encoder can (1) control power settings among payload groups to avoid weak symbols (*e.g.*, the lowest symbol power ≥30 % of the highest symbol); and (2) distribute p-CSS symbols uniformly in frequency bins of the whole spectrum.

Intuitively, we may set frequency guards among p-CSS symbols to protect them from interference. For instance, we can reserve the Least Significant Bit (LSB) of symbols for guard interval to ensure a minimum frequency gap of 2 FFT bins. However, it would lose one bit for all p-CSS symbols, *i.e.*, only the high-order bits are used to encode data, resulting in low encoding efficiency.

HyLink handles the problem in two steps: After encoding N groups of payload data to PHY symbols using standard LoRa encoders, it first detects inter-payload interference among symbols in each chirp duration. If the frequency gaps between some symbols are closer than a guard interval (*e.g.*, 2 FFT bins), HyLink tries to keep only one symbol in the current frequency bin and shift other
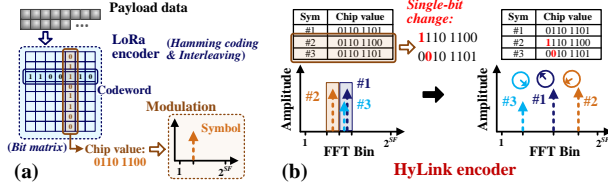
Figure 10: (a) LoRa coding scheme; (b) Resolving inter-payload interference.

symbols to new bins. After that, we can expect all symbols are distributed apart with sufficient frequency gaps.

However, this method encounters technical challenges in practice: While we shift symbols to new frequency bins, it changes the bit encoding of symbols. A receiver may decode incorrect bits from the shifted symbols. It is non-trivial to resolve interference without affecting the normal decoding of payload data.

HyLink overcomes the problem by leveraging the error correction capability of LoRa encoder/decoder. LoRa adopts a couple of coding techniques (*e.g.*, Hamming coding and interleaving [39]) to protect payload data from bit errors. In particular, the payload data are encoded into bit matrices using a modified version of Hamming code as shown in Figure 10(a), where each row is termed a codeword consisting of data bits and parity bits. Any single-bit error in a codeword can be corrected by a decoder. Moreover, LoRa interleaves the bits of codewords in a matrix and encodes bits from different codewords as a chip value that will be modulated onto the same symbol (see Figure 10(a)). It means that even if all bits of a symbol's chip value are being corrupted, the corrupted bits will be dispersed on different codewords. For each codeword, only one bit is affected, which can be corrected by Hamming code.

We reversely exploit the bit error tolerance of LoRa decoders to resolve inter-payload interference. We find that one-bit change on the chip value of a symbol can shift the symbol far away to a different frequency bin. This one-bit change can indeed be corrected by Hamming code of LoRa decoders (see Figure 10(a)). We exploit the observation to resolve interference by flipping one bit of the chip values of interfering symbols. We choose different bits for different symbols to flip the bit encoding, which can shift nearby symbols to different frequency bins as displayed in Figure 10(b). If we cannot find a single-bit change for a symbol that makes the symbol interference-free (*e.g.*, all new frequency bins are occupied), the symbol will be omitted. A receiver can infer the omitted symbol from non-omitted symbols based on that the omitted symbol and any non-omitted symbols should have one-bit difference.

4.4 Power Allocation

As the transmit power of a HyLink node is shared by N payloads, communication reliability in terms of Symbol Error Rates (SERs) can vary across different payloads depending on their allocated power. This subsection addresses how to allocate power resources among concurrent symbols of N payloads.

A p-CSS symbol can be correctly received if a corresponding frequency peak can be detected by FFT after demodulating the received p-CSS signals. As a frequency peak in FFT accumulates power of all time-domain signal samples, the magnitude of frequency peak is proportionately related to the amplitude of a p-CSS

symbol. As such, the amplitude profiles of p-CSS symbols essentially determine how the power resources are allocated among these symbols. The problem of power allocation becomes how to decide signal amplitudes (*i.e.*, α_i's) for the symbols of N payloads.

A general principle on HyLink power allocation is to ensure that: (1) all p-CSS symbols shall be correctly demodulated, and (2) the payload IDs (*i.e.*, phase and amplitude signatures) of p-CSS symbols shall be reliably detected. According to our empirical studies, the phase and amplitude of a p-CSS symbol can be reliably detected if the frequency peak (*i.e.*, accumulated power in FFT) is at least 3 dB higher than the noise floor. To facilitate the analysis for power allocation of p-CSS symbols, we use *Accumulated Signal power to Noise Ratio (ASNR)* to quantitatively measure the signal quality of a received p-CSS symbol, which is calculated in a way similar to the conventional Signal-to-Noise-Ratio (SNR) [36, 62] as follows.

$$ASNR = 10 \log \frac{\sum_{n=1}^{N_S} P_S(n)}{P_N} \text{ dB,} \tag{8}$$

where P_N represents noise power, $P_S(n)$ denotes the signal power of the nth PHY sample and N_S is the total number of signal samples. As all samples of a symbol are transmitted with the same power (P_S), we can transform Eq.(8) to $ASNR = 10 \log \frac{N_S \cdot P_S}{P_N}$.

In practice, the power allocation of HyLink should make sure that the symbols of all payloads will be received with ASNRs higher than a threshold $ASNR_0$ (*i.e.*, the minimum ASNR desired for HyLink decoding). Taking account of the signal power loss along a physical link, we can infer the minimum-required transmit power of a p-CSS symbol as $P_{min} = P_S(ASNR_0) + P_{loss}$, where P_{loss} is link loss and $P_S(ASNR_0)$ denotes the minimum received signal power of a symbol that is derived from $ASNR_0$ according to Eq.(8). Herein, the amplitude settings of p-CSS symbols (*i.e.*, α_i's) shall satisfy the following constraint.

$$\frac{\min\{\alpha_i\}}{\sum_{n=1}^{N} \alpha_n} \cdot P_{tx} \geq P_{min}, \tag{9}$$

where P_{tx} denotes the overall transmit power of a HyLink node. By default, HyLink adopts a uniform amplitude setting. This can generally deliver the highest data-rates. In practice, one may also non-uniformly allocate power to p-CSS symbols, *e.g.*, based on data importance of different payloads.

4.5 Link Rate Adaptation

HyLink selects PHY data-rates for a link connection adaptively according to the physical channel conditions. In PHY, the data-rate of p-CSS modulation can be tuned by the number of concurrent symbols (*i.e.*, N). As all p-CSS symbols share the transmit power of a HyLink node, the number of symbols modulated by p-CSS shall be configured according to channel conditions to ensure reliable receptions of p-CSS symbols over the links provided.

In Figure 11, we examine the ASNRs of received symbols when transmitting different numbers of symbols concurrently through a link in good channel conditions (*i.e.*, SNR>10 dB). We see that when only one symbol is transmitted (*i.e.*, $N = 1$), the symbol is received with the highest ASNR (*i.e.*, 24 dB). While N increases from 1 to 2, the ASNR of each individual symbol decreases from 24 dB to 14 dB. The per-symbol ASNRs decrease further to 9 dB when eight symbols are transmitted. We can see a trend of decreased ASNRs
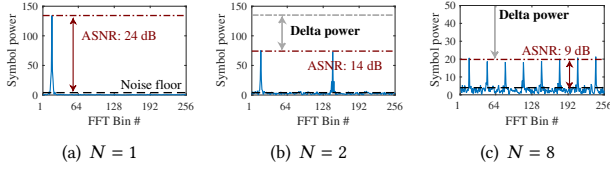
Figure 11: ASNRs of received symbols when different number of symbols are transmitted concurrently.

as more symbols transmit concurrently in PHY. Interestingly, the per-symbol ASNRs decrease dramatically as N increases from 1 to 2, then decrease much slower as N increases to larger numbers. It means that, if a physical channel can support two symbols transmitting concurrently, it is very likely to transmit more concurrent symbols to achieve even higher link throughput.

HyLink fully exploits the channel capability of a link to transmit with the highest PHY data rates allowed by the link. When channel condition is relatively good, HyLink can seize the opportunity by sending multiple chirps (*i.e.*, $N > 1$) together and achieve long-range low-power high-throughput communication. On the other hand, when channel condition becomes poor, HyLink will concentrate all power into a single chirp and conservatively send only one chirp (*i.e.*, $N = 1$) at a time, which can have the same performance of legacy LoRa. Ideally, the number of symbols modulated by p-CSS (*i.e.*, N) should be selected to ensure that all symbols can be reliably received in the current link SNRs. As p-CSS symbols share transmit power of a HyLink node, the per-symbol power constraint provided by Eq.(9) shall be satisfied. Given link SNRs, we can jointly use Eqs.(8) and (9) to derive a coarse estimation on the maximum number of p-CSS modulated symbols (*i.e.*, N_{max}) as below.

$$N_{max} \approx N_s \cdot 10^{(SNR-ASNR_0)/10}, \qquad (10)$$

where N_s is the number of signal samples of a symbol.

To simplify practical operations, HyLink defines a number of Data Rates (DRs) with different SF, BW and N configurations and measures the minimum desired SNRs in prior which is a one-shot effort (refer to Figure 15(b) in §5.2). A HyLink node probes link SNRs at run-time and selects DRs online based on the SNR profiles.

5 EVALUATION

5.1 Methodology

Implementation. We implement HyLink based on a software defined radio platform (USRP N210) and an open source project of LoRa implementation `gr-lora` [18]. HyLink accesses and manipulates the I-Q samples of PHY signals to implement parallel CSS modulation. We reuse the LoRa packet encoder and decoder modules of `gr-lora` and add new GNU Radio modules to implement our HyLink multi-payload encoder and decoder. We note that the current implementation cannot directly run on commodity LoRa nodes because I-Q samples cannot be accessed on commodity devices. If a new-generation LoRa node exposes I-Q samples to higher layers, we can easily implement and run HyLink on those devices.

Testbed. We build a testbed consisting of both HyLink nodes and legacy LoRaWAN devices. We use six USRP N210 devices to run HyLink for performance evaluation. LoRaWAN nodes are composed of commodity Semtech LoRa radios (*i.e.*, SX1276 [42]). We deploy 39
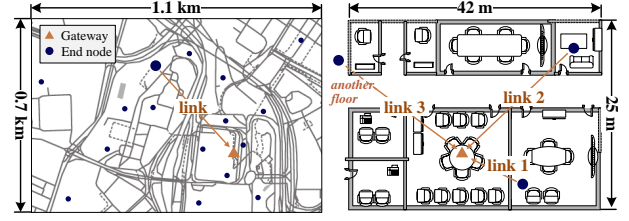

Figure 12: Testbed layout with outdoor (left) and indoor (right) settings.
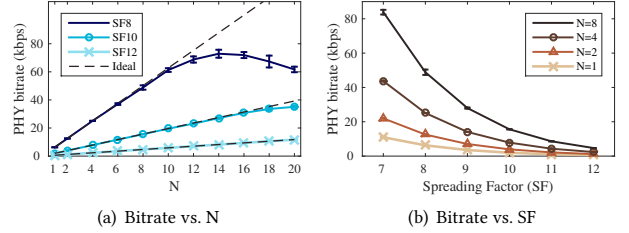

Figure 13: Bitrate gains of HyLink as different numbers of symbols are modulated in PHY (BW: 250 kHz**).**

LoRa nodes in the testbed for link SNR collection and benchmark comparison. The LoRa nodes operate with a 1 % duty cycle and adopt an adaptive data rate scheme recommended by the LoRaWAN standard [34]. The testbed covers a 1.1 km×0.7 km area consisting of indoor and outdoor links as shown in Figure 12. All nodes (HyLink and LoRa) operate in the 915 MHz ISM band.

Experiment setup. We collect data traces for over four months from more than 100 links. The links cover diverse channel conditions in typical urban settings (*e.g.*, buildings, roads, blockages, *etc.*), with SNRs ranging from −10 dB to 25 dB. We apply the traffic profiles (*e.g.*, packet size, communication footprints, SNRs, *etc.*) of collected traces to performance tests of HyLink with practical link settings. We perform extensive experiments to evaluate HyLink, aiming to answer the following questions: (1) How much link capacity can be improved by modulating multiple symbols in PHY? (2) How does HyLink perform in real networks? and (3) How would HyLink affect legacy LoRaWANs? Without otherwise stated, we configure all nodes with the maximum transmit power (20 dBm) and uniformly allocate power among N payloads of HyLink.

Metrics. We evaluate HyLink with three key metrics: (1) *PHY bitrate*: the rate of data bits transferred in the PHY; (2) *Goodput*: the rate of data correctly received by applications; and (3) *Energy per bit*: the energy consumed on successfully transmitting one bit.

5.2 Basic Performance

Gains on link capacity. This experiment evaluates the data-rate gains of HyLink. The signal bandwidth (BW) is 250 kHz. We change the number of symbols modulated by p-CSS (N) and measure PHY bitrates of HyLink nodes in various configurations.

Figure 13(a) presents the measured PHY bitrates under different N settings. We see that the bitrates of SF10 and SF12 linearly increase as more symbols are concurrently modulated. The numbers match well with the theoretic results. The bitrate of SF8 first experiences a linear increase, then reaches the maximum and drops when more than 14 symbols are modulated. It indicates that the
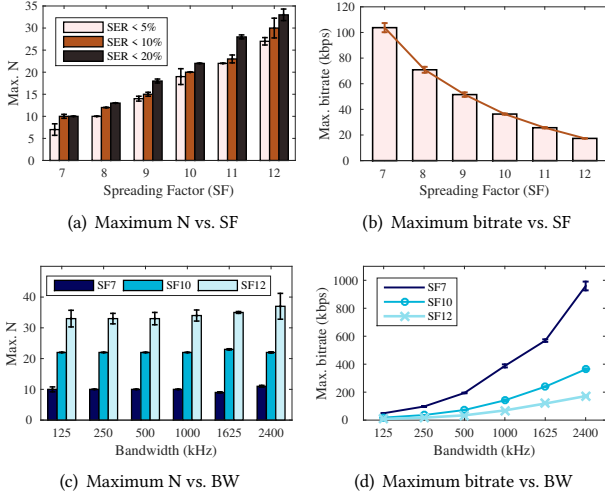
(a) Maximum N vs. SF

(b) Maximum bitrate vs. SF

(c) Maximum N vs. BW

(d) Maximum bitrate vs. BW

Figure 14: Capability on link rate improvement.

maximum number of symbols modulated in PHY would suffer practical limitations. A larger spreading factor generally supports more symbols modulating in the PHY. Figure 13(b) further compares the PHY bitrates under different SF configurations. $N = 1$ corresponds to standard LoRa, which is used as a baseline. As expected, the link capacity increases proportionally with the number of modulated symbols. Generally, a larger N yields higher bitrates for all SFs.

Capability study. We next test the capability of HyLink. We set up links in good SNRs (>5 dB) to examine the largest number of payloads that can be transmitted in a HyLink packet (*i.e.*, the highest number of currently modulated symbols). A payload group of HyLink packet is correctly received if the Symbol Error Rate (SER) of the payload group is lower than a threshold. Figure 14(a) displays the maximum N extracted with different SER thresholds. As expected, we can modulate more concurrent symbols as Spreading Factor (SF) increases. For instance, SF7 supports 10 concurrent symbols; and the number increases to 30 for SF12. Figure 14(b) shows the highest PHY bitrates measured when we modulate the maximum number of symbols for each SF. We see that though a larger SF (*e.g.*, SF12) supports more concurrent symbols, the bitrate is still lower than that of small SF (*e.g.*, SF7). The reason is that a chirp in large SF takes too long time to transmit, which reduces the overall link speed.

Figures 14(c,d) evaluate the impacts of signal bandwidth (BW) on the capability of HyLink. We see that the number of concurrent symbols does not change much across the BW settings. But a high BW parameter reduces the air-time of signal transmission, which can increase PHY bitrates. When BW increases to 2400 kHz, *i.e.*, the largest BW supported by commodity LoRa radios (Semtech SX1280[44]), the bitrate of SF7 increases to as high as 1 Mbps as shown in Figure 14(d).

Impacts of SNR. Figure 15(a) evaluates HyLink performance in different SNRs. In the experiments, we change transmitter and receiver locations to cover a wide range of channel conditions. Comparing the results of −5 dB and >0 dB, we see that a link in high SNRs empowers HyLink to transmit more concurrent symbols. If a link has extremely-low SNR (*e.g.*, −5 dB), transmitting multiple
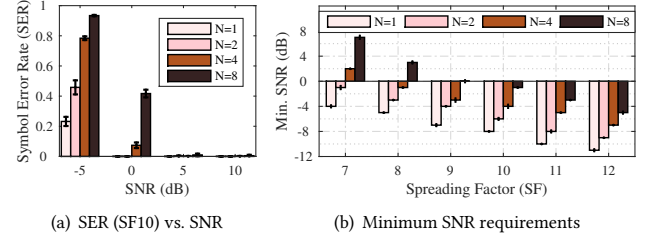

(a) SER (SF10) vs. SNR

(b) Minimum SNR requirements

Figure 15: Interplay between SNR and HyLink.

(a) With a fixed spreading factor (SF10)
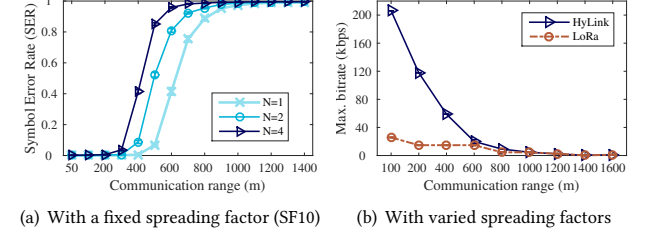
(b) With varied spreading factors

Figure 16: HyLink reception performance (a) and maximum data rates (b) at different communication ranges.

symbols can suffer from high symbol errors. Despite that, even when SNR is as low as 0 dB, we can still reliably transmit four concurrent symbols, which allows HyLink to work on most IoT links (*i.e.*, SNR≥0 dB). Figure 15(b) presents the minimum SNR requirements of HyLink under different settings. We get two observations: (1) Transmitting more concurrent symbols needs higher SNRs; (2) A larger SF can support the same number of concurrent symbols in lower SNRs. We can use the SNR profiles to assist HyLink configurations in practice.

Communication range. This experiment examines the impacts of p-CSS modulation on communication ranges. We use fixed transmission power and ideally estimate the received signal power and SNRs at different communication ranges with a free-space attenuation model. We use the collected traffic traces of corresponding SNR profiles to emulate different communication ranges.

Figure 16(a) evaluates the symbol error rates of HyLink with SF10 and Bandwidth 500 kHz. We see that the longest communication range (*i.e.*, SERs≤20 %) is 500 m when one symbol is modulated (*i.e.*, $N = 1$). The communication range reduces to 400 m and 300 m for $N = 2$ and $N = 4$. This is expected because short ranges generally offer high SNRs, which allows HyLink to transfer more symbols. Next, we adapt CSS (or p-CSS) configurations (*i.e.*, SF and N) according to SNRs and evaluate the maximum data rates of HyLink and LoRa at different communication ranges. As plotted in Figure 16(b), HyLink delivers times higher data rates than LoRa when the ranges are shorter than 400 m. The data-rate improvement decreases as communication ranges increase. Finally, HyLink gives the same data rates as LoRa when the range exceeds 800 m.

Real time performance. Figure 17 examines the time overheads of HyLink on encoding and decoding p-CSS signals of a chirp duration. We normalize encoding/decoding time in relative to the transmission air-time of a chirp. As shown in Figures 17(a) and (b), the longest encoding and decoding time of HyLink are less than 5 % and 55 % of a chirp duration, respectively. The time ratios can

(a) Encoding time per-chirp
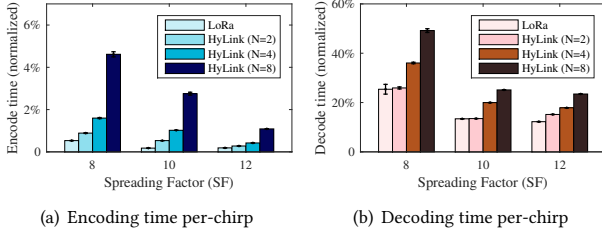
(b) Decoding time per-chirp

Figure 17: Real time performance: encode & decode time are normalized in relative to a chirp duration.

be even lower as SF increases. It means that both the encoding and decoding of p-CSS signals can be completed within the transmission of a chirp signal, indicating good real-time performance.

5.3 Performance in Practical Networks

Controlled experiments with varying traffics. This experiment tests the performance of LoRaWAN and HyLink on satisfying diverse traffic demands. We select three links with low (<0 dB), medium (0~5 dB), and high SNRs (>5 dB) from our indoor testbed as shown in Figure 12. The SNR profiles of the three links cover typical SNR regimes of most links in our testbed. We note that the results of other links look similar but are not displayed due to page limits. We schedule the selected links to communicate 10 s every 1000 s (*i.e.*, duty cycle 1 %) and change traffic rates from 0.001 kbps to 1000 kbps. The links operate in distinctive spreading factors (SF7, SF10 and SF12) according to their SNRs. As SF cannot change arbitrarily due to SNR constraints, we allow LoRaWAN to increase data rates by using a large BW. The largest BWs of link 1 and link 2 are 2.4 MHz, and link 3 is 500 kHz. For fair comparisons, we use the same BW and SF settings for LoRaWAN and HyLink.

Figure 18(a) reports the goodput of LoRaWAN and HyLink. The results validate that LoRaWAN in narrow BW settings can only support low traffic volumes. For instance, due to the poor link SNR and ≤500 kHz BW settings, LoRaWAN delivers at most 0.01 kbps over link 3. The large BW of link 2 can push LoRaWAN's goodput up to 0.1 kbps. Benefiting from both good SNR and large BW, LoRaWAN in link 1 achieves 1 kbps goodput under a 1 % duty-cycle. Similarly, the highest goodput of HyLink is affected by the SNR and BW of physical links. As compared with LoRaWAN, HyLink can boost goodput by one order of magnitude for all three links. The performance gains come from the PHY enhancement on concurrent symbol modulation.

Figure 18(b) evaluates the per-bit energy consumption of LoRaWAN and HyLink in various traffic conditions. We get three observations: (1) For the same traffic condition, links in good SNRs/small SFs (*e.g.*, link 1) consume lower energy than links in poor SNRs/large SFs (*e.g.*, link 3); (2) For the same link, the per-bit energy decreases as a link increases BW to operate in higher data rate (*e.g.*, link 2); and (3) The per-bit energy of HyLink is one order of magnitude lower than that of LoRaWAN. In summary, a link in high data-rate (*e.g.*, links with good SNRs, small SF, large BW and HyLink) can increase energy efficiency because a fast link shortens the transmission time of packets and radio's active time.
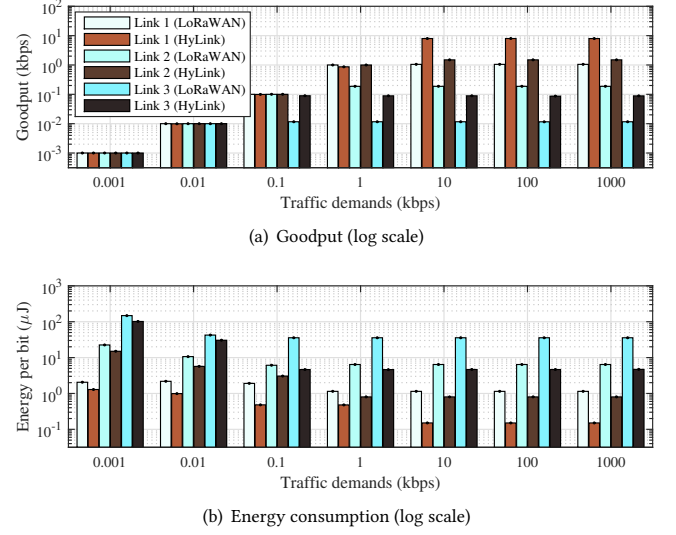

(a) Goodput (log scale)

(b) Energy consumption (log scale)

Figure 18: Performance comparisons of LoRaWAN and HyLink in various traffic conditions (Duty Cycle: 1 %).
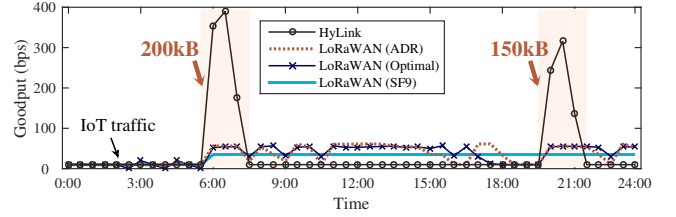

Figure 19: Link performance with practical traffics and SNR settings (BW: 250 kHz, Duty Cycle: 1 %).

Rate adaptation. In this experiment, we test the rate adaptation performance of HyLink with practical link settings. We collect 24-hour traffic traces of a link from our outdoor testbed (see Figure 12) where the SNRs of the link vary over time in −5 dB~15 dB. The transmitter node of the link generates IoT traffics at a rate of 10 bps. It wakes up every 30 minutes to send or receive with a duty cycle of 1 %. The bandwidth (BW) of LoRa packet is 250 kHz. We replay the traces offline on a computer with simulations to ensure fair comparisons among different strategies.

We compare HyLink against three benchmarks: (1) LoRaWAN (SF9) — LoRaWAN with a fixed spreading factor (*i.e.*, SF9) which is the default setting of the link in our testbed; (2) LoRaWAN (Optimal) — LoRaWAN with the optimal SFs selecting dynamically based on link SNRs (using a method similar to [31]); and (3) LoRaWAN (ADR) — an Adaptive Data Rate (ADR) strategy recommended by LoRaWAN [34, 42]. To ensure fair comparisons, we measure link SNRs from the collected raw traffics and replay them with different strategies using the same SNR profiles. We additionally inject two large traffics (*i.e.*, 200 kB at 6:00 and 150 kB at 20:00) to mimic the behaviors of traffic-intensive IoT services (*e.g.*, firmware update [20] and log data collection). If the traffics cannot be finished in a slot, they will be put in a pending queue and scheduled to transfer in the following slots.
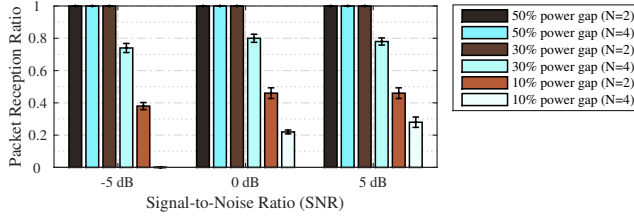
Figure 20: Performance of commodity LoRa nodes on receiving HyLink packets (SF12, BW250 kHz).

Link #1	Link #2	SER #1	SER #2
LoRa (SF7)	LoRa (SF8)	0.0 % (±0)	0.0 % (±0)
LoRa (SF8)	HyLink (SF7, N=2)	0.0 % (±0)	1.2 % (±1.5)
LoRa (SF8)	HyLink (SF7, N=4)	0.0 % (±0)	7.7 % (±5.8)
HyLink (SF7, N=2)	HyLink (SF8, N=2)	1.1 % (±0.9)	1.2 % (±1.2)
HyLink (SF7, N=4)	HyLink (SF8, N=4)	7.5 % (±6.9)	2.4 % (±1.3)
HyLink (SF7, N=4)	*N/A*	2.9 % (±1.8)	*N/A*
HyLink (SF8, N=4)	*N/A*	2.0 % (±1.5)	*N/A*

Table 1: Performance of concurrent communication in orthogonal parameters.

Concurrent links	Packet configurations	SER
#1	LoRa (SF8, BW250 kHz)	1.3 % (±0.7)
#2	HyLink (SF8, BW250 kHz, N=2)	3.9 % (±2.2)
#3	HyLink (SF8, BW250 kHz, N=4)	6.6 % (±4.3)

Table 2: Performance of parallel decoding (PCube [57]) for concurrent HyLink packets in non-orthogonal parameters.

We measure the goodput obtained in each slot and present the results in Figure 19. We see that all strategies can support the regular IoT traffics before 6:00. As a 200 kB data is injected, the link rapidly gets saturated at low goodput levels when LoRaWAN (SF9) is adopted, which prevents the link from serving normal IoT traffics in all the slots after 6:00. When LoRaWAN (Optimal) and ADR are used, the goodputs are higher than that of LoRaWAN (SF9) and fluctuate across slots due to dynamic changes of link SNRs. But we can still observe saturated link capacity in slots ranging from 6:00 to 18:00. This is essentially limited by the link capacity of LoRa PHY. The LoRaWAN (Optimal) and ADR complete the injected large traffic volumes at about 18:00 and then the link recovers from traffic saturation, resulting in lower goodputs than LoRaWAN (SF9) in some slots after 18:00. In contrast, HyLink can adapt link capacity to the increasing traffic demands and boost goodput from 10 bps up to near 400 bps (*i.e.*, 40×). It takes three slots only to complete all injected traffics and recovers soon to serve normal IoT traffics.

5.4 Inter-operation with Legacy LoRa

Backward compatibility. As LoRa packets correspond to a special case of HyLink packets when $N = 1$, a HyLink node can effortlessly receive from legacy LoRa nodes or send a packet to LoRa nodes by encoding only one payload in the packet. In this experiment, we focus on the performance of using LoRa nodes to receive HyLink packets when more than one payload is encoded. We use USRPs to send HyLink packets (SF12, BW250 kHz) and use commodity LoRa nodes with Semtech SX1276 radio to receive. As LoRa nodes decode only one payload from a packet, we allocate higher power to the payload decoding by LoRa node than other payloads. We are specifically interested in how the power gap settings impact the reception performance of LoRa nodes. We change the power settings of HyLink and measure the Packet Reception Ratio (PRR) of LoRa nodes in various SNRs.

Figure 20 presents the packet reception performance of LoRa nodes. We see that legacy LoRa nodes can successfully receive a target payload from HyLink packets ($N > 1$) when the power gap between the target payload and other payloads is large (*e.g.*, 50 %). The PRR drops as the power gaps become small (*e.g.*, 10 %). In addition to power gaps, the PRR can also be affected by the total number of payloads (*i.e.*, N). For instance, a 30 % power gap can ensure 100 % PRRs of the target LoRa payload when $N = 2$. But the PRR drops to around 80 % when $N = 4$. Generally, the power gap shall be larger when more payloads are encoded.

Concurrent communication. Next, we examine HyLink performance in the presence of concurrent communications. We set

up two links transferring simultaneously with different Spreading Factors (SFs) as listed in Table 1. The bandwidth (BW) is fixed to 125 kHz. We measure the Symbol Error Rate (SER) of each link and present the results in Table 1. The SERs of LoRa concurrent communication are displayed for baseline comparison. We see that HyLink can communicate concurrently with either HyLink or legacy LoRa packets as long as they adopt different SFs. As compared with single-link HyLink communication (*i.e.*, the last two rows of Table 1), concurrent HyLink communications yield slightly higher SERs. It can be caused by the imperfect orthogonality of signals [4]. Despite that, the highest symbol errors stay lower than 10 %, which can be corrected by upper-layer encoding schemes (*e.g.*, Hamming code). The results indicate that the orthogonality of underlying CSS modulation parameters (*e.g.*, SF) remain effective for HyLink.

Parallel decoding for HyLink. This experiment studies whether existing parallel decoders can be applied to HyLink. We set up three links to transmit LoRa and HyLink packets concurrently with the same SF and BW parameters as listed in Table 2. All three links have good SNRs (*i.e.*, >10 dB). We choose PCube [57] as our parallel decoder and use two synchronized USRPs as a PCube receiver. The decoding results are presented in the last column of Table 2. We see that PCube works well for HyLink packets. Although a HyLink packet transmits multiple symbols concurrently which increases the number of symbols in the physical channel, all theses symbols can be received and demodulated by PCube receiver, thanks to the good link SNRs and powerful demodulation capability of PCube. PCube can successfully extract the channel features of different links to separate symbols for different packets, and next use either a LoRa decoder or HyLink decoder to decode the separated symbols. It means that HyLink can also be scaled to a large network. In fact, communication concurrency of a network is primarily determined by a parallel decoder. If the total number of concurrent symbols exceeds the demodulation capability of parallel decoder (*e.g.*, PCube), the decoding performance may decrease. Essentially, as the high throughput of HyLink reduces packet air time, it can decrease packet collisions in a network, which would improve communication efficiency and network scalability.

6 DISCUSSION

Communication range. Generally, the SNRs of a link decrease as the communication distance increases, which may reduce the room for data rate improvements for HyLink. Thanks to the rate adaptation capability of p-CSS, HyLink is capable of flexibly tuning data rates according to the SNRs of provided links. If a link is of long-range or poor SNRs, HyLink can modulate fewer symbols with p-CSS (*i.e.*, decrease *N*) or even converts back to LoRa (*i.e.*, *N* = 1) to combat the low SNRs. Therefore, the working range of HyLink remains the same as LoRa. In case a long-range link still offers sufficiently high SNRs, HyLink can grasp the opportunity to improve link throughput by modulating more symbols in PHY.

Approaches to high-throughput LPWAN. As the data rate of LoRa is limited by the narrow bandwidth and long symbol duration of CSS modulation, a possible method for increasing throughput is to increase bandwidth or decrease symbol length. For instance, standard LoRa uses short symbols (*i.e.*, small SFs) to support high data rates. A new LoRa radio SX1280 uses 1.6 MHz bandwidth to achieve a maximum data rate of 254 kbps with CSS. An alternative approach is to adopt new PHY modulation techniques, *e.g.*, FSK and OFDM. NB-IoT, 5G, LET-M and LET Cat-1 belong to this category. However, SX1280 is power-hungry and consumes more spectrum resources. New PHY techniques need to replace deployed LoRa nodes with new radios that would incur high hardware costs. By contrast, HyLink is compatible with legacy LoRa. It can use the available spectrum and radio resources of existing LoRa devices and provide a new dimension for data rate improvement.

7 RELATED WORK

Our research is related to link rate adaptation. The Semtech SX127x radio series [42] are capable of adjusting the Modulation and Coding Scheme (MCS) to support Adaptive Data Rate (ADR) control for LoRa. The LoRaWAN standard [34] recommends a network-managed ADR scheme which requires a central server to configure data rates for end LoRa nodes. It has been implemented on an open-source network manager of TTN (*i.e.*, The Things Network) [50]. ADR strategies have also been proposed in the literature to meet different objectives of LPWANs [12, 29, 63]. DyLoRa [31] employs a model-driven method to estimate the channel conditions of a link and adjust data rates accordingly to improve energy efficiency. Abdelfadeel *et al.* [3] develop algorithms to control transmission power to fairly configure data-rate for end-nodes. Amichi *et al.* [4] consider the imperfect orthogonality of LoRa Spreading Factors (SFs) and jointly allocate SF and Transmit Power to improve throughput, fairness and power performance. More works can be found in [17, 27, 37, 38]. Existing ADR strategies, however, can only adjust data-rate in a limited range due to constraints of the LoRa PHY. They cannot improve capacity for a LoRa link.

Another category focuses on link performance optimization. Chime [13] selects optimal operating frequencies for LoRa links to maximize the data rates and power efficiency. Charm [9] and Choir [10] allow multiple gateways to coherently combine received signals to strengthen signal quality, which can transform to data-rate gains. OPR [5] combines the corrupted packets of multiple receivers to restore a packet at link layer. LMAC [15] reduces packet collisions at a MAC layer to increase goodput of LoRa links. Nephalai

[33] takes a different approach by applying compressive sensing to the LoRa PHY to reduce link bandwidth overheads. NELoRa[30] develops a neural-enhanced demodulator. Unlike these works, our work aims to increase link capacity for LoRa.

HyLink is inspired by the latest advances on LoRa collision resolving [8, 10, 19, 21–24, 45, 52, 53, 56–60]. Recent studies (*e.g.*, Choir [10], NScale [52], CIC [45], PCube [57]) have shown that a LoRa gateway is capable of decoding the collided symbols of different transmitters (*i.e.*, concurrent transmissions), which can increase throughput for the whole network. ==Different from collision resolving, HyLink aims to increase the communication capacity of a single link==. PCube [57] measures the phase of air-channels for collision resolving with multiple antennas and supports concurrent transmissions of multiple LoRa transmitters. Unlike PCube [57], HyLink uses the phase of base-band signals to distinguish different payloads. Thus, the phase extraction method of PCube cannot be applied to HyLink. Besides, HyLink does not need multiple antennas in phase extraction.

Industrial efforts have also been devoted to increasing link capacity for LPWANs. Semtech has released a new product SX1280 which uses more radio resources (*e.g.*, 2.4 MHz bandwidth) to increase LoRa bit rates up to 254 kbps [44]. SX1280 may adopt new modulation techniques, *e.g.*, Fast Long Range Communication (FLRC) and Gaussian Frequency Shift Keying (GFSK), to achieve Mbps bit rates. 3GPP introduces LTE-M [2] and LTE Cat-1 [1] to support medium-speed IoT applications (*e.g.*, at Mbps). More PHY techniques (*e.g.*, Iris [16], NetScatter [19], WiChronos [41], Falcon[51], *etc.*) have been proposed by the academia to optimize LPWANs for longer communication range, lower power consumption or better scalability. In contrast to existing works, HyLink is backward-compatible to existing LoRaWANs and can efficiently use the available spectrum of LoRa and channel capability to provide both high link throughput and low power consumption.

8 CONCLUSION

In this paper, we present HyLink — a cross layer extension to LoRa. HyLink fully exploits the channel capability of high-SNR links to modulate more than one symbol and tunes the number of modulated symbols to adapt link throughput according to channel conditions. HyLink overcomes several practical challenges to ensure reliable communication of multiple payloads in the same packet. Experiments demonstrate that HyLink can transmit in higher throughput and lower power consumption than LoRa in good channels and perform the same with legacy LoRa in poor channels. It is promising to expand LoRa from low-traffic IoT scenarios to a new regime of applications driven by medium- and high-volume traffics.

9 ACKNOWLEDGEMENT

REFERENCES

[1] 3GPP. 2022. *LTE ue-Category*. Retrieved Feb 13, 2022 from https://www.3gpp.org/keywords-acronyms/1612-ue-category

[2] 3GPP. 2022. *The Cellular Internet of Things*. Retrieved Feb 13, 2022 from https://www.3gpp.org/news-events/3gpp-news/1906-c_iot

[3] Khaled Q. Abdelfadeel, Victor Cionca, and Dirk Pesch. 2018. Fair Adaptive Data Rate Allocation and Power Control in LoRaWAN. In *2018 IEEE 19th International Symposium on "A World of Wireless, Mobile and Multimedia Networks" (WoWMoM)*. 14–15.

[4] Licia Amichi, Megumi Kaneko, Ellen Hidemi Fukuda, Nancy El Rachkidy, and Alexandre Guitton. 2020. Joint Allocation Strategies of Power and Spreading Factors With Imperfect Orthogonality in LoRa Networks. *IEEE Transactions on Communications* 68, 6 (2020), 3750–3765.

[5] Artur Balanuta, Nuno Pereira, Swarun Kumar, and Anthony Rowe. 2020. A Cloud-Optimized Link Layer for Low-Power Wide-Area Networks. In *Proceedings of the 18th International Conference on Mobile Systems, Applications, and Services* (Toronto, Canada) *(MobiSys '20)*. Association for Computing Machinery, New York, NY, USA, 247–259.

[6] C. Bernier, F. Dehmas, and N. Deparis. 2020. Low Complexity LoRa Frame Synchronization for Ultra-Low Power Software-Defined Radios. *IEEE Transactions on Communications* 68, 5 (2020), 3140–3152. https://doi.org/10.1109/TCOMM.2020.2974464

[7] BOSCH. 2022. *Fire & Smoke Detection Camera - AVIOTEC IP starlight 8000*. Retrieved Jun 15, 2022 from https://www.boschsecurity.com/xc/en/solutions/fire-alarm-systems/fire-and-smoke-detection-camera/

[8] Qian Chen and Jiliang Wang. 2021. AlignTrack: Push the Limit of LoRa Collision Decoding. In *2021 IEEE 29th International Conference on Network Protocols (ICNP)*. 1–11.

[9] Adwait Dongare, Revathy Narayanan, Akshay Gadre, Anh Luong, Artur Balanuta, Swarun Kumar, Bob Iannucci, and Anthony Rowe. 2018. Charm: exploiting geographical diversity through coherent combining in low-power wide-area networks. In *2018 17th ACM/IEEE International Conference on Information Processing in Sensor Networks (IPSN'18)*. IEEE, 60–71.

[10] R. Eletreby, D. Zhang, S. Kumar, and O. Yagan. 2017. Empowering Low-Power Wide Area Networks in Urban Settings. In *Proceedings of the Conference of the ACM Special Interest Group on Data Communication (SIGCOMM'17)*. 309–321.

[11] Enterprise IoT insights. 2021. *LoRa shoots for 75% of IoT market, versus 25% for 5G; aims for stars with satellite constellation*. Retrieved Oct 13, 2021 from https://enterpriseiotinsights.com/20190618/channels/news/lora-shoots-for-75pc-of-iot-market

[12] Joseph Finnegan, Ronan Farrell, and Stephen Brown. 2020. Analysis and Enhancement of the LoRaWAN Adaptive Data Rate Scheme. *IEEE Internet of Things Journal* 7, 8 (2020), 7171–7180.

[13] Akshay Gadre, Revathy Narayanan, Anh Luong, Anthony Rowe, Bob Iannucci, and Swarun Kumar. 2020. Frequency configuration for low-power wide-area networks in a heartbeat. In *17th USENIX Symposium on Networked Systems Design and Implementation (NSDI'20)*. 339–352.

[14] Akshay Gadre, Fan Yi, Anthony Rowe, Bob Iannucci, and Swarun Kumar. 2020. Quick (and Dirty) Aggregate Queries on Low-Power WANs. In *2020 19th ACM/IEEE International Conference on Information Processing in Sensor Networks (IPSN)*. 277–288. https://doi.org/10.1109/IPSN48710.2020.00031

[15] Amalinda Gamage, Jansen Christian Liando, Chaojie Gu, Rui Tan, and Mo Li. 2020. *LMAC: Efficient Carrier-Sense Multiple Access for LoRa*. Association for Computing Machinery, New York, NY, USA.

[16] Chuhan Gao, Mehrdad Hessar, Krishna Chintalapudi, and Bodhi Priyantha. 2019. Blind Distributed MU-MIMO for IoT Networking over VHF Narrowband Spectrum. In *The 25th Annual International Conference on Mobile Computing and Networking* (Los Cabos, Mexico) *(MobiCom '19)*. Association for Computing Machinery, New York, NY, USA, Article 26, 17 pages.

[17] Weifeng Gao, Wan Du, Zhiwei Zhao, Geyong Min, and Mukesh Singhal. 2019. Towards Energy-Fairness in LoRa Networks. In *2019 IEEE 39th International Conference on Distributed Computing Systems (ICDCS)*. 788–798.

[18] Gr-LoRa GitHub community. 2021. *gr-lora projects*. Retrieved Mar 15, 2021 from https://github.com/rpp0/gr-lora

[19] Mehrdad Hessar, Ali Najafi, and Shyamnath Gollakota. 2019. Netscatter: Enabling large-scale backscatter networks. In *16th USENIX Symposium on Networked Systems Design and Implementation (NSDI'19)*. 271–284.

[20] Mehrdad Hessar, Ali Najafi, Vikram Iyer, and Shyamnath Gollakota. 2020. TinySDR: Low-Power SDR Platform for Over-the-Air Programmable IoT Testbeds. In *17th USENIX Symposium on Networked Systems Design and Implementation (NSDI 20)*. USENIX Association, Santa Clara, CA, 1031–1046. https://www.usenix.org/conference/nsdi20/presentation/hessar

[21] Ningning Hou, Xianjin Xia, and Yuanqing Zheng. 2021. Jamming of LoRa PHY and Countermeasure. In *IEEE INFOCOM 2021 - IEEE Conference on Computer Communications*. 1–10. https://doi.org/10.1109/INFOCOM42981.2021.9488774

[22] Ningning Hou, Xianjin Xia, and Yuanqing Zheng. 2022. Don't Miss Weak Packets: Boosting LoRa Reception with Antenna Diversities. In *IEEE INFOCOM 2022 - IEEE Conference on Computer Communications*. 530–539. https://doi.org/10.1109/INFOCOM48880.2022.9796699

[23] Bin Hu, Zhimeng Yin, Shuai Wang, Zhuqing Xu, and Tian He. 2020. SCLoRa: Leveraging Multi-Dimensionality in Decoding Collided LoRa Transmissions. In *2020 IEEE 28th International Conference on Network Protocols (ICNP'20)*. IEEE, 1–11.

[24] Qianyi Huang, Zhiqing Luo, Jin Zhang, Wei Wang, and Qian Zhang. 2020. LoRadar: Enabling Concurrent Radar Sensing and LoRa Communication. *IEEE Transactions on Mobile Computing* (2020), 1–1. https://doi.org/10.1109/TMC.2020.3035797

[25] Industryarc.com. 2021. *LoRa and LoRaWAN Devices Market Overview*. Retrieved Oct 13, 2021 from https://www.industryarc.com/Report/19424/lora-and-lorawan-devices-market.html

[26] Dhananjay Jagtap and Pannuto Pat. 2021. Repurposing Cathodic Protection Systems as Reliable, in-Situ, Ambient Batteries for Sensor Networks. In *Proceedings of the 20th International Conference on Information Processing in Sensor Networks (Co-Located with CPS-IoT Week 2021)* (Nashville, TN, USA) *(IPSN '21)*. Association for Computing Machinery, New York, NY, USA, 357–368. https://doi.org/10.1145/3412382.3458277

[27] Zerina Kapetanovic, Deepak Vasisht, Tusher Chakraborty, Joshua R. Smith, and Ranveer Chandra. 2021. No Size Fits All: Automated Radio Configuration for LPWANs. https://doi.org/10.48550/ARXIV.2109.05103

[28] Daniel Kiv, Garvita Allabadi, Berkay Kaplan, and Robin Kravets. 2022. Smol: Sensing Soil Moisture Using LoRa *(LP-IoT'21)*. Association for Computing Machinery, New York, NY, USA, 21–27.

[29] Rachel Kufakunesu, Gerhard P. Hancke, and Adnan M. Abu-Mahfouz. 2020. A Survey on Adaptive Data Rate Optimization in LoRaWAN: Recent Solutions and Major Challenges. *Sensors* 20, 18 (2020). https://doi.org/10.3390/s20185044

[30] Chenning Li, Hanqing Guo, Shuai Tong, Xiao Zeng, Zhichao Cao, Mi Zhang, Qiben Yan, Li Xiao, Jiliang Wang, and Yunhao Liu. 2021. NELoRa: Towards Ultra-Low SNR LoRa Communication with Neural-Enhanced Demodulation. In *Proceedings of the 19th ACM Conference on Embedded Networked Sensor Systems* (Coimbra, Portugal) *(SenSys '21)*. Association for Computing Machinery, New York, NY, USA, 56–68.

[31] Yinghui Li, Jing Yang, and Jiliang Wang. 2020. DyLoRa: Towards Energy Efficient Dynamic LoRa Transmission Control. In *IEEE INFOCOM 2020 - IEEE Conference on Computer Communications*. 2312–2320.

[32] Jansen C. Liando, Amalinda Gamage, Agustinus W. Tengourtius, and Mo Li. 2019. Known and Unknown Facts of LoRa: Experiences from a Large-Scale Measurement Study. *ACM Trans. Sen. Netw.* 15, 2, Article 16 (feb 2019), 35 pages. https://doi.org/10.1145/3293534

[33] Jun Liu, Weitao Xu, Sanjay Jha, and Wen Hu. 2020. *Nephalai: Towards LPWAN C-RAN with Physical Layer Compression*. Association for Computing Machinery, New York, NY, USA.

[34] LoRa Alliance. 2021. *LoRaWAN for Developer*. Retrieved Jun 24, 2021 from https://lora-alliance.org/lorawan-for-developers

[35] MarketsAndMarkets. 2021. *Low Power Wide Area Network Market by Connectivity Technology (SIGFOX, LoRaWAN, Weigthless and Others), Technology Service, Network Deployment, Application, Verticals and Region - Global Forecast to 2021*. Retrieved Nov 13, 2021 from https://www.marketsandmarkets.com/Market-Reports/low-power-wide-area-network-market-41351212.html

[36] Lionel M Ni, Yunhao Liu, Yiu Cho Lau, and Abhishek P Patil. 2004. LANDMARC: Indoor location sensing using active RFID. *Wireless Networks* 10, 6 (2004), 701–710.

[37] Gopika Premsankar, Bissan Ghaddar, Mariusz Slabicki, and Mario Di Francesco. 2020. Optimal Configuration of LoRa Networks in Smart Cities. *IEEE Transactions on Industrial Informatics* 16, 12 (2020), 7243–7254.

[38] Brecht Reynders, Wannes Meert, and Sofie Pollin. 2017. Power and spreading factor control in low power wide area networks. In *2017 IEEE International Conference on Communications (ICC)*. 1–6.

[39] Pieter Robyns, Peter Quax, Wim Lamotte, and William Thenaers. 2018. A Multi-Channel Software Decoder for the LoRa Modulation Scheme. In *Proceedings of International Conference on Internet of Things, Big Data and Security (IoTBDS)*. 41–51.

[40] Martijn Saelens, Jeroen Hoebeke, Adnan Shahid, and Eli De Poorter. 2019. Impact of EU duty cycle and transmission power limitations for sub-GHz LPWAN SRDs: an overview and future challenges. *EURASIP Journal on Wireless Communications and Networking* 2019, 219 (2019), 1–32.

[41] Yaman Sangar and Bhuvana Krishnaswamy. 2020. *WiChronos: Energy-Efficient Modulation for Long-Range, Large-Scale Wireless Networks*. Association for Computing Machinery, New York, NY, USA.

[42] Semtech. 2021. *Semtech SX1276: 137MHz to 1020MHz Long Range Low Power Transceiver*. Retrieved Jun 25, 2021 from https://www.semtech.com/products/wireless-rf/lora-transceivers/sx1276

[43] Semtech. 2021. *Updating Firmware Over-the-Air*. Retrieved Oct 17, 2021 from https://lora-developers.semtech.com/documentation/tech-papers-and-guides/firmware-updates-over-the-air

[44] Semtech. 2022. *LoRa 2.4GHz*. Retrieved Jan 30, 2022 from https://www.semtech.com/products/wireless-rf/lora-24ghz

[45] Muhammad Osama Shahid, Millan Philipose, Krishna Chintalapudi, Suman Banerjee, and Bhuvana Krishnaswamy. 2021. Concurrent Interference Cancellation: Decoding Multi-Packet Collisions in LoRa *(SIGCOMM '21)*. Association for Computing Machinery, New York, NY, USA.

[46] Sigfox. 2022. *SIGFOX, THE 0G NETWORK CONNECTING YOUR PHYSICAL WORLD*. Retrieved Mar 13, 2022 from https://www.sigfox.com/en

[47] statista. 2021. *Number of LPWAN connections by technology worldwide from 2017 to 2023*. Retrieved Oct 13, 2021 from https://www.statista.com/statistics/880822/lpwan-ic-market-share-by-technology/

[48] Zehua Sun, Huanqi Yang, Kai Liu, Zhimeng Yin, Zhenjiang Li, and Weitao Xu. 2022. Recent Advances in LoRa: A Comprehensive Survey. *ACM Trans. Sen. Netw.* (jun 2022). https://doi.org/10.1145/3543856 Just Accepted.

[49] Jothi Prasanna Shanmuga Sundara, Wan Du, and Zhiwei Zhao. 2019. A Survey on LoRa Networking: Research Problems, Current Solutions, and Open Issues. *IEEE Communications Surveys & Tutorials* 22, 1 (2019), 371–388.

[50] The Things Network. 2022. *The Things Network*. Retrieved Feb 11, 2022 from https://www.thethingsnetwork.org/

[51] Shuai Tong, Zilin Shen, Yunhao Liu, and Jiliang Wang. 2021. *Combating Link Dynamics for Reliable Lora Connection in Urban Settings*. Association for Computing Machinery, New York, NY, USA, 642–655.

[52] Shuai Tong, Jiliang Wang, and Yunhao Liu. 2020. Combating Packet Collisions Using Non-Stationary Signal Scaling in LPWANs. In *Proceedings of the 18th International Conference on Mobile Systems, Applications, and Services (MobiSys '20)*. 234–246.

[53] Shuai Tong, Zhenqiang Xu, and Jiliang Wang. 2020. CoLoRa: Enabling Multi-Packet Reception in LoRa. In *IEEE INFOCOM 2020 - IEEE Conference on Computer Communications*. 2303–2311.

[54] Galini Tsoukaneri, Franscisco Garcia, and Mahesh K. Marina. 2020. Narrowband IoT Device Energy Consumption Characterization and Optimizations. In *Proceedings of the 2020 International Conference on Embedded Wireless Systems and Networks on Proceedings of the 2020 International Conference on Embedded*

[55] The Things Network (TTN). 2022. *LoRaWAN distance world record broken, twice. 766 km (476 miles) using 25mW transmission power*. Retrieved Jun 17, 2022 from https://www.thethingsnetwork.org/article/lorawan-distance-world-record

[56] Zhe Wang, Linghe Kong, Kangjie Xu, Liang He, Kaishun Wu, and Guihai Chen. 2020. Online Concurrent Transmissions at LoRa Gateway. In *IEEE INFOCOM 2020 - IEEE Conference on Computer Communications*. 2331–2340.

[57] Xianjin Xia, Ningning Hou, Yuanqing Zheng, and Tao Gu. 2021. PCube: Scaling LoRa Concurrent Transmissions with Reception Diversities. In *Proceedings of the 27th Annual International Conference on Mobile Computing and Networking (MobiCom'21)*. ACM.

[58] Xianjin Xia, Yuanqing Zheng, and Tao Gu. 2020. LiteNap: Downclocking LoRa Reception. In *IEEE INFOCOM 2020 - IEEE Conference on Computer Communications*. 2321–2330. https://doi.org/10.1109/INFOCOM41043.2020.9155224

[59] Xianjin Xia, Yuanqing Zheng, and Tao Gu. 2019. FTrack: Parallel Decoding for LoRa Transmissions *(SenSys '19)*. Association for Computing Machinery, New York, NY, USA.

[60] Zhenqiang Xu, Pengjin Xie, and Jiliang Wang. 2021. Pyramid: Real-Time LoRa Collision Decoding with Peak Tracking. In *IEEE INFOCOM 2021 - IEEE Conference on Computer Communications*. 1–9.

[61] Deliang Yang, Xianghui Zhang, Xuan Huang, Liqian Shen, Jun Huang, Xiangmao Chang, and Guoliang Xing. 2020. *Understanding Power Consumption of NB-IoT in the Wild: Tool and Large-Scale Measurement*. Association for Computing Machinery, New York, NY, USA.

[62] Zheng Yang, Zimu Zhou, and Yunhao Liu. 2013. From RSSI to CSI: Indoor localization via channel response. *ACM Computing Surveys (CSUR)* 46, 2 (2013), 1–32.

[63] Qihao Zhou, Jinyu Xing, Lu Hou, Rongtao Xu, and Kan Zheng. 2019. A Novel Rate and Channel Control Scheme Based on Data Extraction Rate for LoRa Networks. In *2019 IEEE Wireless Communications and Networking Conference (WCNC)*. 1–6.